CANCER

Prediction of immunotherapy response using mutations to cancer protein assemblies

JungHo Kong[1], Xiaoyu Zhao[1], Akshat Singhal[2], Sungjoon Park[1], Robin Bachelder[1], Jeanne Shen[3], Haiyu Zhang[3], Jimin Moon[4], Changho Ahn[4], Chan-Young Ock[4], Hannah Carter[1]*, Trey Ideker[1,2,5]*

While immune checkpoint inhibitors have revolutionized cancer therapy, many patients exhibit poor outcomes. Here, we show immunotherapy responses in bladder and non–small cell lung cancers are effectively predicted by factoring tumor mutation burden (TMB) into burdens on specific protein assemblies. This approach identifies 13 protein assemblies for which the assembly-level mutation burden (AMB) predicts treatment outcomes, which can be combined to powerfully separate responders from nonresponders in multiple cohorts (e.g., 76% versus 37% bladder cancer 1-year survival). These results are corroborated by (i) engineered disruptions in the predictive assemblies, which modulate immunotherapy response in mice, and (ii) histochemistry showing that predicted responders have elevated inflammation. The 13 assemblies have diverse roles in DNA damage checkpoints, oxidative stress, or Janus kinase/signal transducers and activators of transcription signaling and include unexpected genes (e.g., PIK3CG and FOXP1) for which mutation affects treatment response. This study provides a roadmap for using tumor cell biology to factor mutational effects on immune response.

INTRODUCTION

Immune checkpoint inhibitors (ICI) have come to the forefront as a promising therapy for patients with cancer (*1*), as they have been associated with longer-lasting clinical benefits, prolonged survival, and fewer side effects than standard chemotherapies. However, only a fraction of patients (e.g., 15 to 30% in solid tumors) attain these milestones, and ICI treatment is sometimes accompanied by toxicity, autoimmune reactions, or life-threatening adverse events such as pneumonitis (*2*–*4*). Accordingly, active research programs are underway to identify biomarkers predictive of ICI response (*5*–*10*), with the goals of elucidating resistance mechanisms and developing therapies that target resistance pathways (*11*, *12*).

Tumor mutation burden (TMB), typically quantified as the number of nonsynonymous somatic mutations per megabase in the tumor genome, was an early biomarker associated with ICI response (*13*). Across tumor types, a general relationship was reported between high TMB and objective response rates to immunotherapy, with melanoma and colorectal cancers with microsatellite instability having some of the best outcomes (*14*). This and other reports (*15*) led to accelerated approval by the US Food and Drug Administration to treat high TMB tumors with pembrolizumab, an ICI therapy that blocks the programmed cell death protein 1 (PD-1) receptor on the surface of T cells (*1*).

Since that time, the use of TMB as a biomarker has become increasingly controversial. One study found that TMB levels failed to show predictive accuracy in glioma, prostate, and breast cancers (*16*), while another reported that, contrary to expectations, low TMB is paradoxically associated with longer survival in ICI-treated glioblastoma (*17*). These and other (*17*, *18*) incongruous results suggest the need to better understand the complex relationships among ICI, TMB, and tumor response.

One factor that may limit the utility of TMB is that it provides a relatively coarse measure of the potential of genetic disruptions to trigger an immune response. High TMB is thought to serve as a proxy for a higher burden of neoantigens, though several studies have suggested that the quality of neoantigens is more important than quantity (*19*–*21*). In this respect, tumors carrying somatic mutations in certain oncogenic pathways, or mutations interfering with effective antigen presentation, have been associated with particularly poor response rates (*22*, *23*). Examples include mutations affecting *CTNNB1*, *APC*, *AXIN1*, and *TCF1* in the β-catenin signaling pathway (*24*), or mutations within the mammalian target of rapamycin (mTOR) or epidermal growth factor receptor pathways (*25*–*28*), all of which have been associated with resistance to ICI treatment. Moreover, three separate studies (*18*, *29*, *30*) have reported that patients with non–small cell lung cancer (NSCLC) with mutations in major histocompatibility class I (MHC-I) genes have impaired antigen presentation leading to poor ICI responses, even in the context of high TMB. ICI response has also been linked to genetic alterations in Janus kinase (JAK) proteins (*31*), which are known for their roles in regulating immune cytokines, as well as in other signaling pathways related to leukocyte and T cell proliferation (*32*).

Such studies suggest that the influence of TMB on response to immunotherapy depends on at least two distinct forces. The first force relates to global immunogenicity, wherein tumors with a high number of somatic mutations tend to produce abundant neoantigens. The second force relates to the local effects of mutations on specific cancer functions. Certain mutations, such as inactivating mutations to the MHC-I pathway, can promote tumor viability and thus counteract the global effect of immunogenicity.

Here, we report that factoring mutational burden by these two separate aspects can enable improved prediction of ICI response (Fig. 1A). Our approach is to assess the specific mutational burdens on many multi-genic subcellular components, informed by a map of known and candidate tumor protein assemblies documented to be

[1]Department of Medicine and Moores Cancer Center, School of Medicine, University of California San Diego, San Diego, CA, USA. [2]Department of Computer Science and Engineering, University of California San Diego, San Diego, CA, USA. [3]Department of Pathology, Stanford University School of Medicine, Stanford, CA, USA. [4]Lunit Incorporated, Seoul, South Korea. [5]Department of Bioengineering, University of California San Diego, San Diego, CA, USA.
*Corresponding author. Email: hkcarter@health.ucsd.edu (H.C.); tideker@health.ucsd.edu (T.I.)

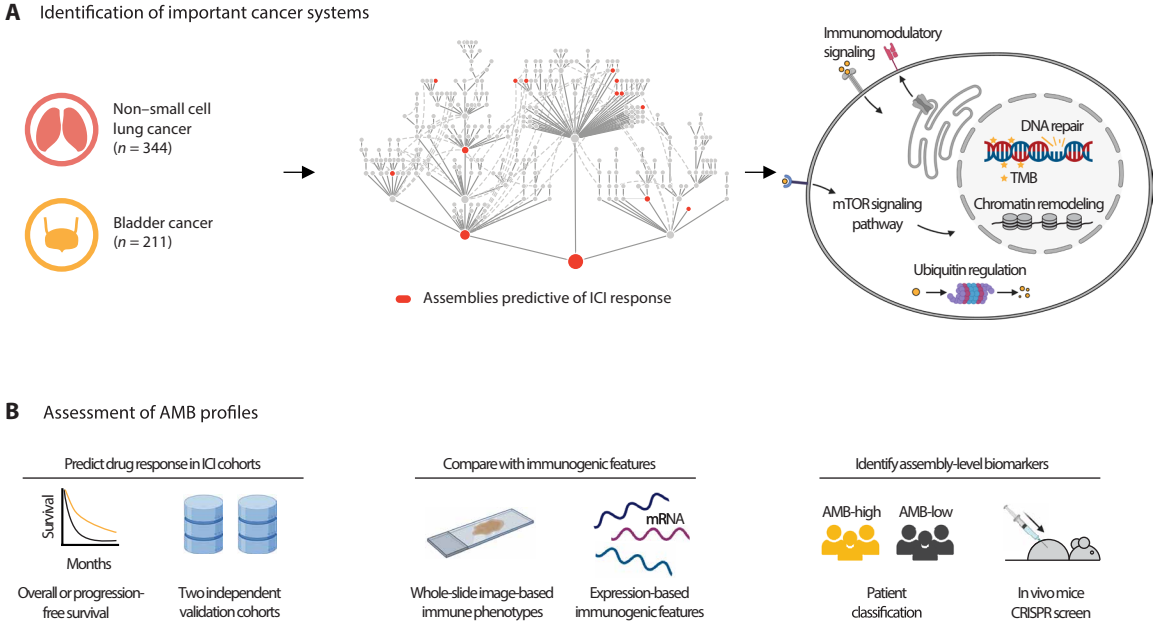

Fig. 1. Identifying mutated protein assemblies as biomarkers of ICI response. (**A**) Immunotherapy-treated patients are analyzed by computing somatic mutation burdens across a hierarchy of known and putative physical assemblies of proteins. Counts (*n*) refer to the number of patients in the Samstein discovery cohort (see text). This analysis reveals a constellation of protein assemblies for which the assembly-level mutation burden (AMB) is predictive of treatment outcomes. (**B**) The predictive power of the AMB profile is assessed using survival data in two independent validation cohorts. In addition, the AMB-derived risk score is compared to immunogenic phenotypes from tumor histopathology imaging and mRNA expression levels of tumor biopsies (middle), then further validated by CRISPR screens in mice (right).

under selective pressure in adult cancers (*33*). By assessing the TMB in combination with this profile of assembly-level mutation burdens (AMBs), we identify a constellation of informative ICI response biomarkers that can be corroborated by independent genetic perturbations in mice, evidence of immune infiltration in histology samples, and validation in patients (Fig. 1B).

RESULTS

Formulation of immunotherapy data

We focused on ICI response prediction in NSCLC and bladder cancers (BLCA), as both tumor types have been approved for ICI treatment, and response data have been released as a single integrated cohort (NSCLC, $n = 344$; BLCA, $n = 211$) (Samstein cohort) (*34*). In this dataset, tumors were subjected to mutational profiling for 468 cancer-related genes comprising the MSK-IMPACT gene panel (Memorial Sloan Kettering Integrated Mutation Profiling of Actionable Cancer Targets), with immunotherapy outcomes measured as overall patient survival. We found no statistical differences in mutation rates between patients with NSCLC and BLCA ($P = 0.19$; fig. S1A). Mutational analysis indicated that known genetic biomarkers of ICI response (*22*) were mutated infrequently in this cohort (e.g., 3% of tumors with JAK3 mutation; Fig. 2A), with the exceptions of TP53 (57.1%) and KRAS (23.6%). For validation, we obtained separate collections of ICI-treated NSCLC tumors from Hellmann *et al.* (*35*) ($n = 68$) and BLCA tumors from the IMvigor210 trial (*11*) ($n = 78$). In the independent validation cohorts, all tumors had been subjected to genome-wide mutational profiling, with immunotherapy outcomes reported as well as progression-free survival (PFS; Hellmann cohort) or overall survival (OS; IMvigor210).

Computation of local mutation burdens on protein assemblies

We developed a methodology to predict ICI response using local mutational burdens observed in specific molecular complexes in tumor cells. For this purpose, we downloaded the collection of 394 cancer protein assemblies provided by the "Nested Systems in Tumors" (NeST) cell map (*33*). These assemblies had been generated by comprehensive measurement of physical protein-protein interactions centered on 61 proteins that are frequently altered in solid tumor types, followed by integration of these data with numerous previous proteomics studies to create a large cancer protein interaction network. Structural analysis of this network revealed a hierarchy of protein assemblies in which small, specific complexes of cancer proteins nest within larger communities corresponding to broad processes and organelles. We observed that 85 of these assemblies were commonly mutated, defined as assemblies for which >20% of tumors in the Samstein cohort had mutations in one or more proteins (Fig. 2B). Each Samstein tumor was thus assigned an AMB for each of the 394 assemblies, with AMB defined simply as the total count of assembly proteins with somatic coding mutations (see Materials and Methods; Fig. 2C). The profile of AMB values for all assemblies was used to train a predictive random forest model of patient response after ICI treatment, yielding a predicted "AMB risk" score, with higher risk indicating lower tendency to respond to ICI and predicted as nonresponders (see Materials and Methods).

Assembly-level mutation burden predicts immunotherapy response

We first evaluated the performance of the AMB risk score in predicting the OS by conducting leave-one-out cross-validation in the

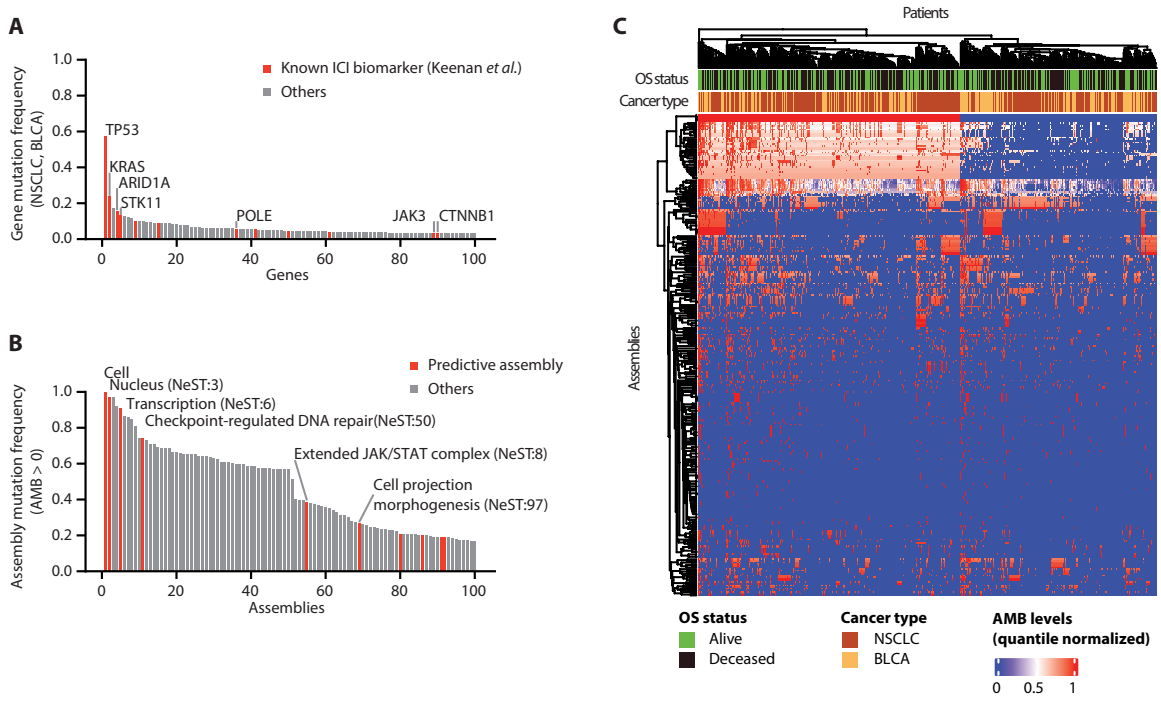

Fig. 2. Local mutational burdens converge on protein assemblies. (**A**) Mutation frequencies of the top 100 most frequently altered genes in the Samstein BLCA and NSCLC cohorts ($N = 555$). Previously reported ICI biomarkers curated by Keenan *et al.* (*22*) are shown in red. (**B**) Mutation frequencies of the top 100 most frequently altered protein assemblies in the same cohorts as (A). Assemblies predictive of ICI response are shown in red. (**C**) AMB landscape for all 394 assemblies (rows) across 555 tumor samples (columns) from the Samstein cohort. AMBs for each assembly are quantile normalized, with a blue-to-red color scale indicating low to high mutation burdens, respectively. Overall survival (OS) status is also shown (green and black indicating alive and deceased, respectively). Hierarchical clustering is applied to both rows and columns, with corresponding dendrograms shown.

Samstein cohort and selecting the top 20% with the lowest predicted AMB risk as responders and others as nonresponders (see Materials and Methods). This analysis revealed a significant difference in survival between predicted responders and nonresponders ($P = 3.39 \times 10^{-5}$; Fig. 3A), associated with a hazard ratio of 0.51 (95% confidence interval: 0.37 to 0.71). Qualitatively, similar results were observed using an alternative performance metric and cross-validation method [concordance index (CI) with Monte Carlo cross-validation; Fig. 3B]. We then compared the AMB risk score to current biomarker models that use TMB alone (Cox proportional hazard model) or individual gene-level mutation burdens (GMB; random forest). The AMB risk showed improved performance over TMB ($P = 2.04 \times 10^{-7}$; Fig. 3B). To provide a negative control for these findings, we repeated this analysis by randomly permuting the assignment of mutated genes to protein assemblies. This random permutation led to a substantial deterioration in predictive performance, indicating that the specific factorization of genes into commonly mutated assemblies was important for accurate prediction (Fig. 3C).

Validation in independent cohorts

To assess the generalizability of AMB risk predictions, we used the previously trained model to predict the response status of patients in the independent NSCLC Hellmann cohort (*35*) described above, without any additional optimization or parameter tuning (see Materials and Methods). From principal components analysis, we found that AMB profiles were well correlated between the Samstein and Hellmann or IMvigor210 cohorts, without evidence of batch effects (fig. S1, B and C). We examined if AMB risk could be used to predict this quantitative PFS outcome in the Hellmann cohort. We found that predicted responders exhibited substantially longer PFS than predicted nonresponders (high AMB risk, $P = 3.74 \times 10^{-4}$; Fig. 3D); this predictive performance was on par or better than TMB (Fig. 3E) or GMB (Fig. 3F). We also investigated predictive performance in a second independent cancer cohort (patients with IMvigor210 BLCA, described above). Here too, we found that predicted IMvigor210 responders showed longer OS compared to predicted nonresponders ($P = 2.48 \times 10^{-2}$; Fig. 3G), outperforming TMB (Fig. 3H) or GMB (Fig. 3I). Collectively, these results suggested that integrating the mutational burden within specific protein assemblies offers a promising strategy for understanding the response to ICIs.

Unraveling protein assemblies predictive of treatment response

We next moved from predictive performance to molecular interpretation, seeking to identify and study the specific protein assemblies in which genetic alterations were most important for model predictions. For this purpose, among the 394 assemblies, we identified 13 core assemblies that were assigned high importance during model training (see Materials and Methods; z-score ≥ 1.6; fig. S2A). These important assemblies spanned a wide range of sizes, with functions related to checkpoint-regulated DNA repair, regulation of expression via SWI/SNF chromatin remodeling, ubiquitin regulation, the mTOR pathway, and an extended JAK/signal transducers and activators of transcription (STAT) signaling complex (Fig. 4A and

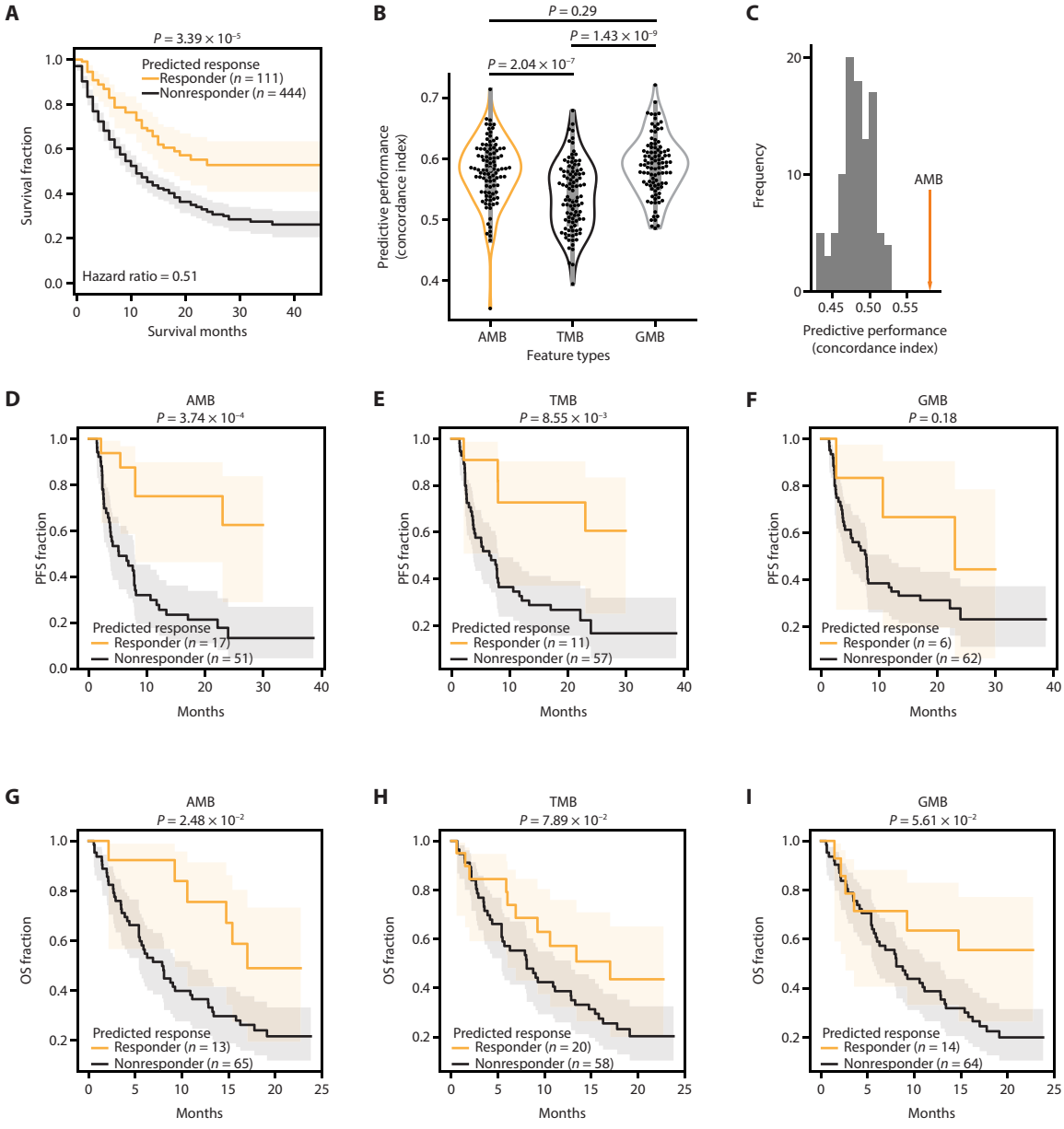

Fig. 3. Predictive performance of ICI models. (**A**) Performance of ICI response prediction in the Samstein cohort using AMB scores, assessed using leave-one-out cross-validation. The log-rank test is used to compute statistical significance. (**B**) Performance of ICI response prediction in the Samstein cohort, using different types of mutation burden as features: AMB, overall TMB, and gene-level mutation burden (GMB). Cross-validation using 90% of the Samstein dataset as training ($n = 499$) and 10% as testing ($n = 56$) over 100 independent random partitions (see Materials and Methods). Performance is measured using the concordance index (CI) between risk scores and survival. Statistical significance was measured using the Mann-Whitney *U* test. (**C**) Predictive performance of a population of randomized controls ($n = 100$) in which gene-assembly relationships have been randomly permuted. (**D** to **F**) Predictive performance in the Hellmann cohort. Prediction of PFS using (D) AMB, (E) TMB, or (F) GMB. Log-rank test to compute statistical significance. (**G** to **I**) Predictive performance in the IMvigor210 cohort.

fig. S2, A and B). Alterations in six of these assemblies, including checkpoint-regulated DNA repair (NeST:50) and the extended JAK/STAT complex (NeST:8), were associated with sensitivity to ICI treatment (see Materials and Methods; Fig. 4A). The remaining seven important assemblies, including ubiquitin regulation of oxidative stress (NeST:230), were associated with resistance (Fig. 4A). Some of the assemblies were encoded by genes with previously identified roles in immunotherapy response (fig. S2C) (*22*). In particular, checkpoint-regulated DNA repair had the highest enrichment for known genomic determinants of ICI response (hypergeometric test, $P < 10^{-2}$). This assembly encompassed components of mismatch repair (MSH2 and MSH6) and cell-cycle control (CDK4 and CDK6), which have been previously linked to the regulation of programmed death ligand 1 (PD-L1) (*22*, *36*). The remaining assemblies had moderate to low enrichment for previously documented markers of ICI response (fig. S2C).

Next, we tested if the importance of assemblies to ICI response, as determined above, could be corroborated by gene knockout (KO)

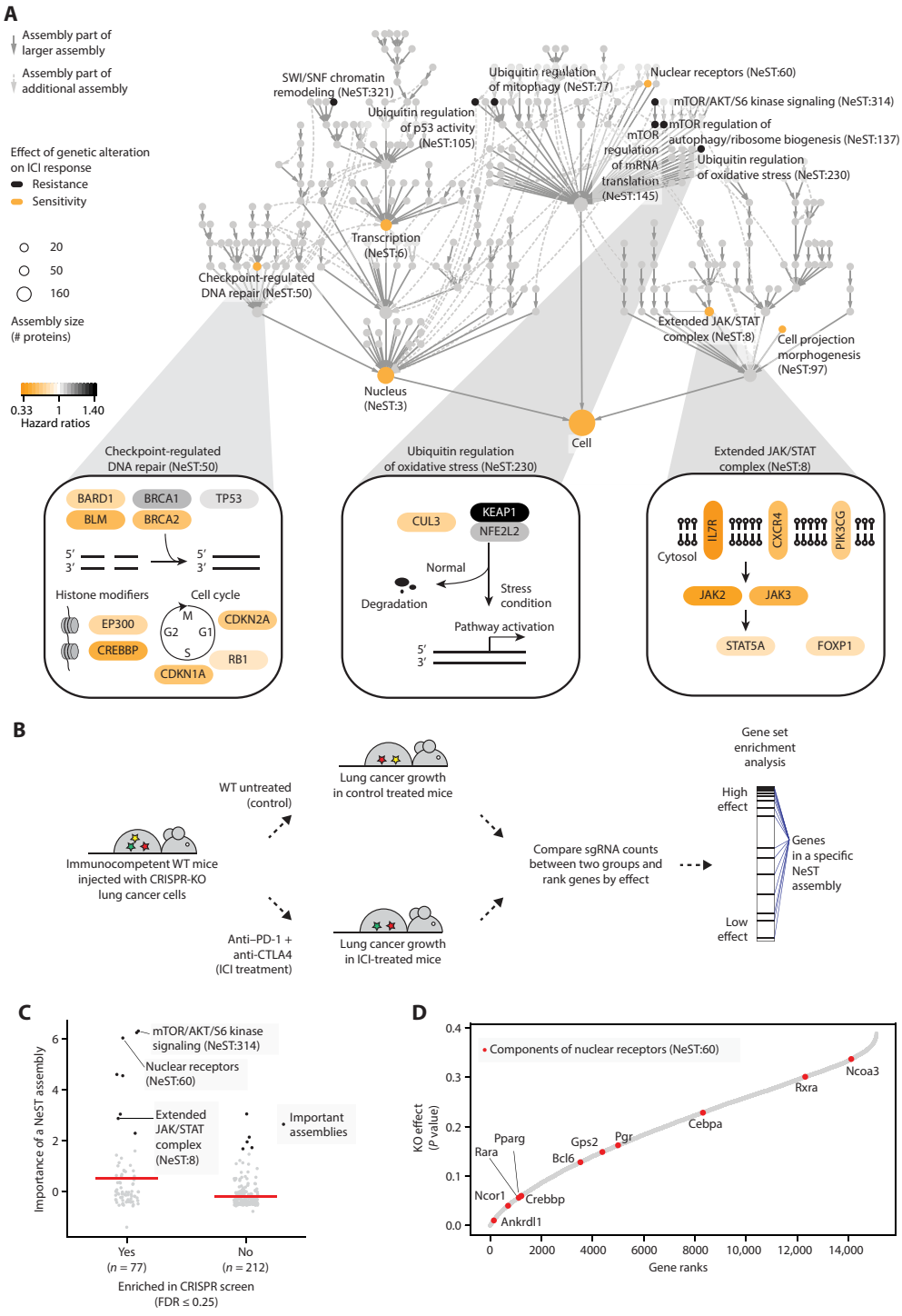

Fig. 4. Important protein assemblies in ICI response prediction. (**A**) The hierarchy shows the NeST compendium of protein assemblies (*33*). Nodes represent assemblies, and node size indicates assembly size in a number of proteins. Colors indicate assemblies scoring as important for ICI response prediction, with black and yellow indicating resistance and sensitivity, respectively. Edges indicate containment relationships (of one assembly by another) whereby a smaller assembly occurs within a larger one. Three predictive assemblies are detailed at the bottom. For each gene, the yellow-to-black color scale is based on the importance of genetic alterations to that gene in the Samstein dataset, determined using the hazard ratio of resistance. Pathway figures are adapted from NDEx IQuery (*71*, *72*). (**B**) In vivo CRISPR screening of genome-wide gene knockouts (KO; for each of 15,105 genes) in lung cancer cells injected in immunocompetent mice (*37*). Mice were grouped by anti–PD-1 plus anti-CTLA4 treatment or no immunotherapy treatment to measure the effects of gene KO on immunotherapy efficacy. WT, wild type. (**C**) Comparison of model importance scores between NeST assemblies enriched or not enriched in in vivo CRISPR screening. Black dots indicate important assemblies. Red horizontal bars indicate mean importance scores. FDR, false discovery rate. (**D**) KO effects of NeST:60 components (red dots). Genes are ranked by their KO effects on tumor growth, where a lower rank indicates a higher effect.

experiments (Fig. 4, B and C). For this purpose, we analyzed data from a recent genome-wide CRISPR screen (*37*), in which gene KOs had been ranked by their absolute effects on lung tumor growth in ICI-treated versus control groups of mice (i.e., considering effects in either direction, with highly ranked genes either increasing or decreasing tumor growth; Fig. 4B). We observed that 8 of the 13 important assemblies were enriched for high-effect gene KOs (false discovery rate of 0.25; see Materials and Methods; Fig. 4C), showing a significant enrichment (Fisher's exact test $P = 0.0072$; data S4). Important assemblies with high KO effect included mTOR/AKT/S6 kinase signaling (NeST:314), a cluster associated with nuclear receptors (NeST:60) and the extended JAK/STAT complex (NeST:8) (Fig. 4C). Notable examples in the NeST:60 nuclear receptor cluster include genes with known roles in tumor immunosurveillance, such as Nuclear Receptor Co-Repressor 1 (Ncor1) (*38*) and CREB-binding protein (Crebbp) (*12*), as well as genes with unexpected roles in cancer immune response such as Ankyrin Repeat Domain-Like 1 (Ankrdl1), Retinoic Acid Receptor Alpha (Rara), and Peroxisome Proliferator-Activated Receptor Gamma (Pparg), all of which showed strong KO effects on tumor growth (Fig. 4D).

Protein assemblies predict immune infiltration

One of the hallmarks of a successful ICI response is tumor immunogenicity, the degree to which a tumor is primed to provoke a reaction from the patient's immune system (*39*). We thus investigated whether patients with low AMB risk showed characteristic immune phenotypes, such as the presence of tumor-infiltrating lymphocytes (TILs). For this purpose, we analyzed 804 patients with NSCLC for which both tumor genomic alteration profiles and hematoxylin and eosin–stained histology images had been generated by The Cancer Genome Atlas project (TCGA-LUAD and TCGA-LUSC) (*40*, *41*). Histology images were processed using a previously developed deep learning system that leverages ResNet-34 (*39*). By this approach, individual cells are first identified in the image by type (cancer, stroma, or lymphocyte), then broader regions of the image are classified as "inflamed" (high density of intraepithelial TILs), "excluded" (lymphocytes detected only within tumor stromal regions), or "desert" (lymphocytes not detected) (Fig. 5A and Supplementary Text).

Notably, we observed that patients for which the AMB model had predicted an effective ICI response (AMB low-risk) displayed significantly larger regions of inflammation in the histology images than did AMB high-risk individuals (Mann-Whitney *U* test $P < 0.01$; Fig. 5B). Consistent with this finding, AMB responders also displayed significantly lower regions of immune exclusion (Fig. 5, C and D). In contrast, TMB- and GMB-based classifications were less correlated with immune inflammation (Fig. 5C) and exclusion (Fig. 5D).

To corroborate these results, we performed a complementary analysis of tumor mRNA expression, also available for this TCGA cohort. We adapted a previously described approach to analyze the expression signature of each tumor sample to estimate its relative proportions of T cell lymphocytes and macrophages (see Materials and Methods). Similar to our observations with tumor histology, the immune phenotypes identified from tumor expression analysis showed significant association with AMB risk predictions (Mann-Whitney U test $P < 0.01$; fig. S3, A to E). In contrast, high TMB or GMB showed less correlation with immunosuppressive signatures, including those of regulatory T cell– and tumor-associated macrophages (fig. S3, D and E).

We identified 11 protein assemblies for which mutation burden was particularly associated with histology or expression-based immune phenotypes (see Materials and Methods; fig. S3F). Among these, the mutation burden of NeST:230 was strongly associated with higher lymphocyte exclusion and reduced lymphocyte infiltration (Fig. 5E and fig. S3, G and H). The high association in this case was not the result of mutations to a single gene; rather, it represented the convergence of mutations on a constellation of genes with functions in oxidative stress, including KEAP1, NFE2L2, and CUL3 (Fig. 5E and fig. S4).

JAK/STAT genes are more predictive in aggregate than individually

One of the most important assemblies for ICI response prediction was NeST:8, a complex of 50 proteins with known or candidate roles in JAK/STAT signaling during immunosurveillance ("Extended JAK/STAT assembly"). This assembly was mutated in approximately 38% of ICI-treated patients (Fig. 6A). The AMB score of this assembly was found to accurately stratify patient survival in both the Samstein (Fig. 6B) and the Hellman cohorts (Fig. 6C). Furthermore, alterations to this assembly were linked to higher TILs in the TCGA cohort (Fig. 5E and fig. S3, F and G). In contrast to the AMB, individual factors within this NeST:8 assembly were less frequent (e.g., JAK3, FLT3, or NTRK3; Fig. 6, A and D), leading to less predictive performance when considered individually (Fig. 6E and figs. S4 and S5). For example, previously reported immunotherapy biomarkers in this complex (*22*, *31*, *42*), such as B2M, JAK2, and STAT5A, were mutated very rarely in either Samstein (Fig. 6A) or Hellmann cohorts (<2%) (Fig. 6D). These results support the use of protein assemblies as robust biomarkers of ICI response, as they can have both a high frequency of observation and a significant effect size.

DISCUSSION

In total, our study identified 13 assemblies in which genetic alterations are informative of an effective ICI response. Notably, these assemblies incorporate a wide range of single-gene biomarkers previously reported to inform ICI (*22*) (although not all, see study limitations below). For instance, alterations to DNA repair assemblies (NeST:50 and NeST:3) were strongly associated with increased ICI sensitivity (Fig. 4), consistent with previous reports that loss-of-function mutations in DNA mismatch repair genes sensitize patients to ICI treatment due to an increased TMB (*22*, *43*). A second example is the mTOR pathway, which was implicated in several important assemblies (NeST:137, NeST:145, and NeST:314; Fig. 4) and has been previously associated with the regulation of immune cells, which can affect the efficacy of ICI treatment (*44*, *45*). We also observed that ubiquitin regulation of oxidative stress (NeST:230) is associated with higher lymphocyte exclusion and ICI resistance (Fig. 5E). Supporting these observations, previous studies have reported that loss of KEAP1, one of the frequently mutated components of the ubiquitin regulation of oxidative stress assembly (NeST:230), provides growth advantages in lung cancer (*46*) as well as diminished immunotherapy response (*47*).

The predictive protein assemblies also implicate factors not previously associated with immunotherapy response. For example, alterations in nuclear receptor assembly (NeST:60) were linked with modulating ICI response in human patients (Fig. 4A) and in mice (Fig. 4, B to D). Moreover, alterations to PIK3CG, encoding one of the most frequently mutated members of the extended JAK/STAT

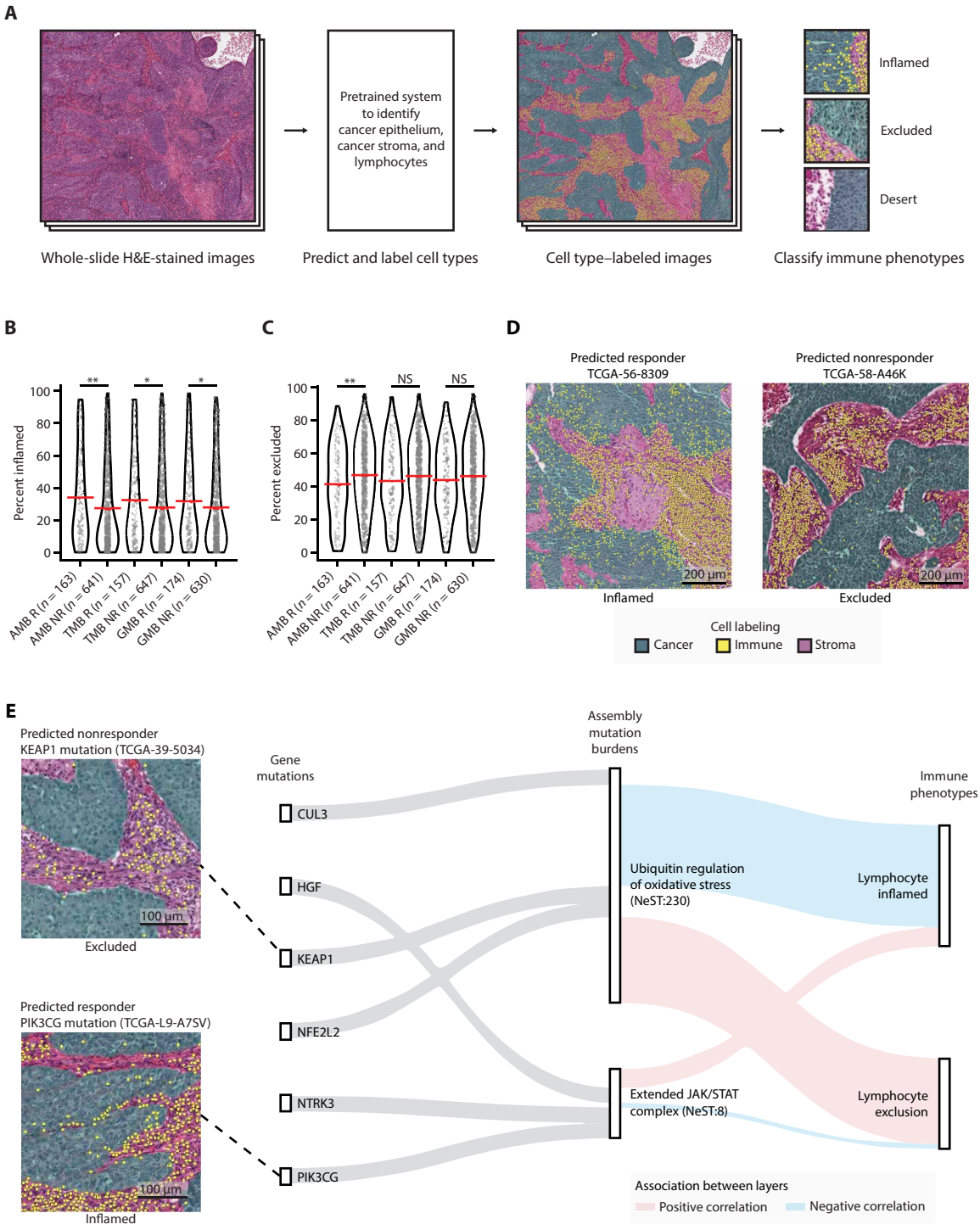

Fig. 5. Immune landscape of patients with predicted high- and low-risk TCGA NSCLC. (**A**) Schematic diagram for labeling cell types in patients with TCGA NSCLC using hematoxylin and eosin (H&E)–stained image data. (**B** and **C**) Association between predicted ICI responses from AMB-, TMB-, or GMB-based predictions, and immune phenotypes from image data. Percent of (B) inflamed or (C) excluded grids (0.25-mm^2 size for each grid) over the total H&E-stained image (see Materials and Methods). Red horizontal bars indicate the mean. Mann-Whitney *U* test was used to compute statistical significance. *$P < 0.05$; **$P < 0.01$; NS, $P > 0.05$. NS, not significant. (**D**) Images from representative specimens for patients predicted by the AMB model as ICI responders (left) or nonresponders (right). Images show inflamed (left) or excluded (right) immune phenotypes. Cells colored green, yellow, and purple indicate cancer epithelium, lymphocytes, and cancer stroma, respectively. (**E**) Sankey diagram showing genetic information flow from mutations in genes (first layer) to AMBs of assemblies (second layer) to immunogenic features (third layer). The top three highly mutated genes (Samstein cohort) in each assembly were selected for display. Feature importance scores [SHapley Additive exPlanations (SHAP) values; see Materials and Methods] are used to highlight associations between layers. Red and blue lines indicate positive and negative associations, respectively.

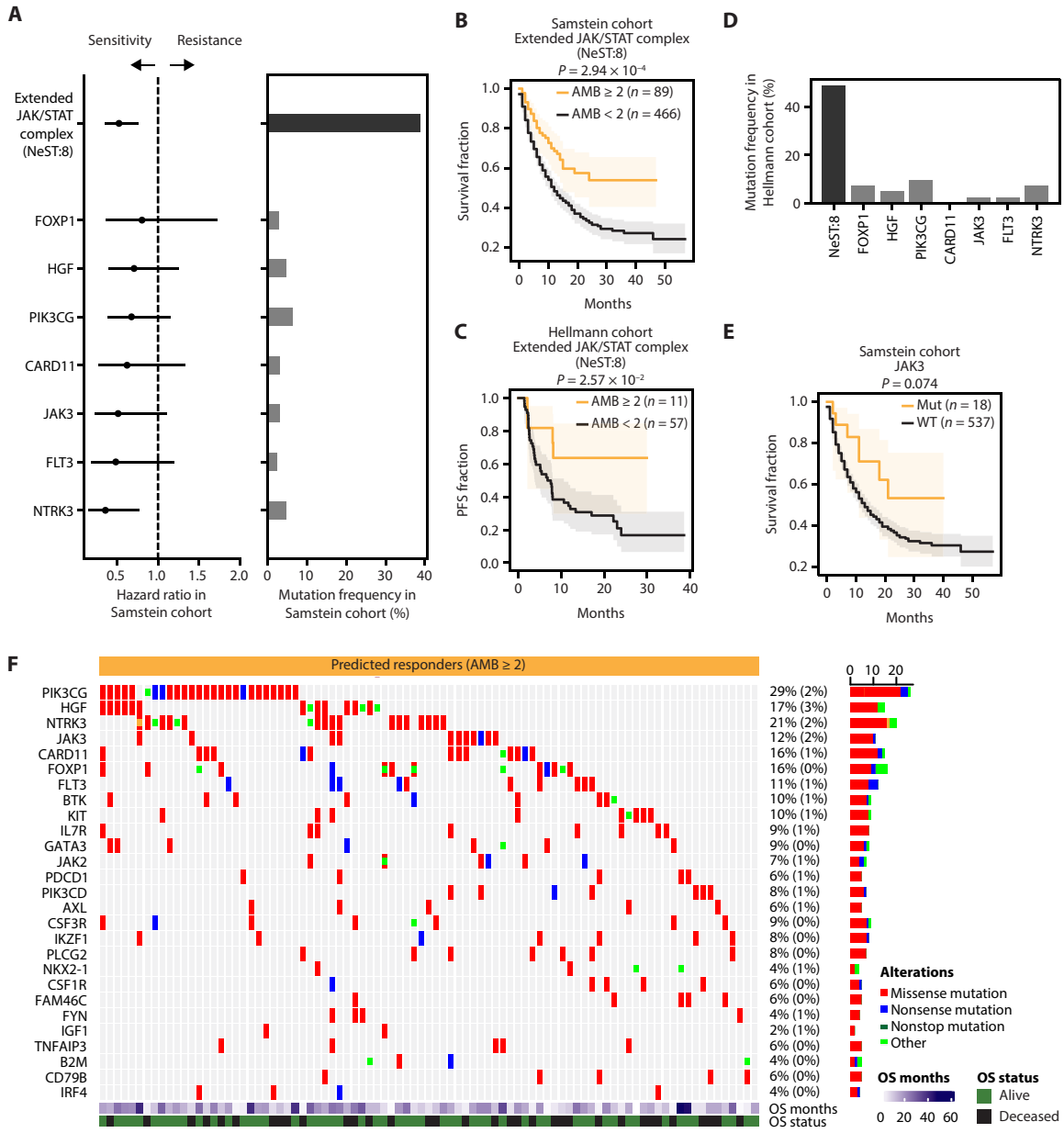

Fig. 6. Mutation burden on an extended JAK/STAT complex predicts ICI response. (**A**) Stratification of ICI response in the Samstein cohort (*x* axis, hazard ratio) by distinct genetic features (*y* axis; left). Features include AMB levels of the NeST:8 assembly (top row) and the presence/absence of mutation in each of its encoding genes (all other rows). AMB ≥ 2 was used to classify patients. Error bars represent 95% confidence intervals. Genes with mutation frequency greater than 3% are displayed. Mutation frequency (*x* axis) for each feature shown on the right. (**B** and **C**) Stratification of ICI-treated patients in (B) the Samstein cohort or (C) the Hellmann cohort using NeST:8 AMB scores. (**D**) Mutation frequency for each feature in the Hellmann cohort. (**E**) Stratification in the Samstein cohort using JAK3 mutations. (**F**) Alteration patterns in patients with NeST:8 AMB ≥ 2 in the Samstein cohort. The color indicates alteration type; "other" includes frameshift insertions/deletions, splice site/region alterations, and in-frame insertions/deletions. Summary mutation frequencies in responders are shown at right as percentages (corresponding mutational frequencies in predicted nonresponders are in parentheses).

complex (Fig. 6F), are associated with both higher sensitivity to treatment (Fig. 6A) and higher lymphocyte infiltration (Fig. 5E). Roles for PIK3CG in immune cell function have been previously reported (*48*, *49*), and it has been reported that this gene is overexpressed and mutated in cancer (*50*–*54*). However, the effects of PIK3CG mutations on tumor cell biology have been little studied (*55*). It is possible that point mutations in PIK3CG alter its enzymatic activity (*56*) and/or enhance G protein–coupled receptor signaling (*55*). In addition, we found that alterations to FOXP1, another component of the NeST:8 complex, are associated with sensitivity to ICI treatment (Fig. 6A). In line with these findings, high levels of FOXP1 have been reported to suppress immune signatures (e.g., MHC-II expression) (*57*), negatively regulate follicular helper T cells (*58*), and associate with lower TILs (*59*).

We acknowledge some limitations of this study. First, because the Samstein cohort conducted targeted sequencing of 468 genes, mutation profiles of some immunotherapy-related genes (e.g., interferon-ɣ,

LAG3, TIGIT, or LILRB2) were not considered. Second, while we have focused on somatic mutation burden, integrating other molecular layers, such as copy number alterations, may improve model performance or interpretability. A previous report found that tumor aneuploidy is associated with diminished immunotherapy response in patients with melanoma (*60*), raising the question of whether the associated genetic copy number changes converge on specific protein assemblies in the same manner as point mutations. Last, while we have leveraged a cancer cell map that was generated across cancer types and tissues (*33*), equivalent maps for noncancer cellular contexts (e.g., immune cells) or specific cancer cell types (*61*–*64*) may provide additional information on responses to ICI treatment.

In summary, we have described a predictive model of ICI response that integrates patterns of tumor mutations with prior biological knowledge of physical protein assemblies. In contrast to studies that use TMB as a proxy for neoantigens (*21*, *65*) or focus on individual gene biomarkers of ICI response (*26*, *28*), a tumor's AMB risk score captures both of these concepts within a hierarchy of large-to-small genetic systems. The result is an expanded collection of immunotherapy biomarkers, as well as a general framework that may extend to other treatment responses.

MATERIALS AND METHODS

Preparation of mutation features

A panel of 468 genes (MSK-IMPACT) was used to assess the mutational impact on response to immunotherapy. We marked each gene as mutated ("1") if it had (i) missense/nonsense mutations, (ii) frameshift insertions/deletions, (iii) splice site regions, or (iv) in-frame insertions/deletions in a patient tumor; otherwise, the gene was marked as unmutated ("0"). To calculate an AMB, we used the gene-to-assembly associations from the NeST hierarchy (*33*). The mutational burden of an assembly was calculated by counting the sum of the number of mutated genes observed in the genes of the assembly. For TMB, we used the reported TMB values for the Samstein (*34*), Hellmann (*35*), and IMvigor210 cohorts (*11*). For IMvigor210 patients, we only considered patients with BLCA and removed samples biopsied before chemotherapy treatment. For TCGA patients, we calculated the TMB using the Maftools R package (*66*).

Model training procedures

OS data in the Samstein cohort were used to train Cox regression (for TMB model) (*67*) and random survival forest models (for AMB and GMB models) (*68*) using lifelines (*69*) and scikit-survival Python packages, respectively (*70*). For random survival forest models, we conducted fivefold cross-validation in the training dataset to identify optimal tree depth (3, 5, 10, or max). We used 500 trees for training, and the log-rank test was used to make splits (*70*). To predict OS in response to ICI therapy, we used risk scores defined as the average cumulative hazard function (CHF) estimates (Nelson-Aalen estimator) of the terminal node of each decision tree (*68*). This average CHF estimate at time t, given input features x, was defined as

$$H(t \mid x) = \frac{1}{B} \sum_{b=1}^{B} \sum_{t} \frac{d_{b,t}}{Y_{b,t}}$$

where B is the number of trees (here $B = 500$) and $d_{b,t}$ and $Y_{b,t}$ are the number of deaths at time t and number of individuals at risk before time t, respectively, with both these quantities relevant to decision tree b.

Model validation procedures

To measure the performance of the AMB model in the Samstein cohort (Fig. 3A), we conducted leave-one-out cross-validation. For this purpose, we designated the top 20% of patients with the lowest predicted risks as "predicted responders" (*34*); the remaining 80% of patients were designated as "predicted nonresponders." We also used the Samstein cohort to conduct Monte Carlo cross-validation (Fig. 3B), whereby we partitioned 90 and 10% of the data into training and test datasets, respectively, for each of the 100 independent iterations. Performance in Monte Carlo cross-validation was measured using the CI. The CI measures, over all admissible patient pairs, the frequency with which the model predicts patient j to outlive i when j outlives i in observed data (*69*). The CI was defined as

$$C = \frac{N_C + 0.5 \times N_T}{N_C + N_D + N_T}$$

where N_C, N_D, and N_T correspond to the number of concordant pairs, discordant pairs, and tied pairs, respectively. CI scores were computed by using the lifelines package where censored information was included when computing CI scores. To measure performance in the validation cohorts (the Hellmann and IMvigor210 cohorts), we determined the optimal tree depth for AMB- and GMB-based models from the Samstein cohort by selecting the most frequently selected tree depth from the Monte Carlo cross-validation (data S1). The tree depths selected were 3 and max tree depths for AMB- and GMB-based models, respectively. To stratify patients into predicted responders and nonresponders in the validation ICI cohorts, we identified a cutoff score from the Samstein cohort. Cutoff scores were determined by the lowest 20% risk score in the Samstein cohort, corresponding to 19.60, 15.55, or 0.90 risk scores for AMB, GMB, or TMB models, respectively.

Identification of important assemblies

To score the importance of each assembly, we computed the decrease in model performance when the AMB value of this assembly was randomly shuffled over the patients in the cohort, with this performance decrease computed for each of the 100 independent iterations. A difference between the original model performance and the average performance of the random models was determined as a feature importance score. Feature importance scores were converted to z-scores (fig. S2A). To nominate important assemblies, we considered assemblies with feature importance scores having $z > 1.64$, corresponding to the 95% confidence level in a one-tailed test (fig. S2A). The hazard ratio using AMB levels of an assembly was used to determine the direction of sensitivity or resistance (Fig. 4A).

Validation of the extended JAK/STAT complex (NeST:8)

Patients were stratified into low-risk and high-risk classes by thresholding the AMB of the "Extended JAK/STAT complex" (NeST:8). We selected an optimal threshold (AMB ≥ 2 for low risk, else high risk) that showed the best predictive performance in the Samstein cohort, as determined by a log-rank test. The same threshold was applied to stratify patients in the Hellmann cohort (Fig. 6C).

Supplementary Materials

This PDF file includes:

Supplementary Text
Figs. S1 to S7
Legends for data S1 to S10
References

Other Supplementary Material for this manuscript includes the following:

Data S1 to S10

REFERENCES AND NOTES

1. A. D. Waldman, J. M. Fritz, M. J. Lenardo, A guide to cancer immunotherapy: From T cell basic science to clinical practice. *Nat. Rev. Immunol.* **20**, 651–668 (2020).
2. Y. Jing, J. Liu, Y. Ye, L. Pan, H. Deng, Y. Wang, Y. Yang, L. Diao, S. H. Lin, G. B. Mills, G. Zhuang, X. Xue, L. Han, Multi-omics prediction of immune-related adverse events during checkpoint immunotherapy. *Nat. Commun.* **11**, 4946 (2020).
3. D. Y. Wang, J.-E. Salem, J. V. Cohen, S. Chandra, C. Menzer, F. Ye, S. Zhao, S. Das, K. E. Beckermann, L. Ha, W. K. Rathmell, K. K. Ancell, J. M. Balko, C. Bowman, E. J. Davis, D. D. Chism, L. Horn, G. V. Long, M. S. Carlino, B. Lebrun-Vignes, Z. Eroglu, J. C. Hassel, A. M. Menzies, J. A. Sosman, R. J. Sullivan, J. J. Moslehi, D. B. Johnson, Fatal toxic effects associated with immune checkpoint inhibitors. *JAMA Oncol.* **4**, 1721–1728 (2018).
4. C. H. June, J. T. Warshauer, J. A. Bluestone, Is autoimmunity the Achilles' heel of cancer immunotherapy? *Nat. Med.* **23**, 540–547 (2017).
5. N. Auslander, G. Zhang, J. S. Lee, D. T. Frederick, B. Miao, T. Moll, T. Tian, Z. Wei, S. Madan, R. J. Sullivan, G. Boland, K. Flaherty, M. Herlyn, E. Ruppin, Robust prediction of response to immune checkpoint blockade therapy in metastatic melanoma. *Nat. Med.* **24**, 1545–1549 (2018).
6. P. Jiang, S. Gu, D. Pan, J. Fu, A. Sahu, X. Hu, Z. Li, N. Traugh, X. Bu, B. Li, J. Liu, G. J. Freeman, M. A. Brown, K. W. Wucherpfennig, X. S. Liu, Signatures of T cell dysfunction and exclusion predict cancer immunotherapy response. *Nat. Med.* **24**, 1550–1558 (2018).
7. A. Bagaev, N. Kotlov, K. Nomie, V. Svekolkin, A. Gafurov, O. Isaeva, N. Osokin, I. Kozlov, F. Frenkel, O. Gancharova, N. Almog, M. Tsiper, R. Ataullakhanov, N. Fowler, Conserved pan-cancer microenvironment subtypes predict response to immunotherapy. *Cancer Cell* **39**, 845–865.e7 (2021).
8. J. S. Lee, N. U. Nair, G. Dinstag, L. Chapman, Y. Chung, K. Wang, S. Sinha, H. Cha, D. Kim, A. V. Schperberg, A. Srinivasan, V. Lazar, E. Rubin, S. Hwang, R. Berger, T. Beker, Z. Ronai, S. Hannenhalli, M. R. Gilbert, R. Kurzrock, S. H. Lee, K. Aldape, E. Ruppin, Synthetic lethality-mediated precision oncology via the tumor transcriptome. *Cell* **184**, 2487–2502.e13 (2021).
9. Ó. Lapuente-Santana, M. van Genderen, P. A. J. Hilbers, F. Finotello, F. Eduati, Interpretable systems biomarkers predict response to immune-checkpoint inhibitors. *Patterns* **2**, 100293 (2021).
10. J. H. Kong, D. Ha, J. Lee, I. Kim, M. Park, S. H. Im, K. Shin, S. Kim, Network-based machine learning approach to predict immunotherapy response in cancer patients. *Nat. Commun.* **13**, 3703 (2022).
11. S. Mariathasan, S. J. Turley, D. Nickles, A. Castiglioni, K. Yuen, Y. Wang, E. E. Kadel, H. Koeppen, J. L. Astarita, R. Cubas, S. Jhunjhunwala, R. Banchereau, Y. Yang, Y. Guan, C. Chalouni, J. Ziai, Y. Şenbabaoğlu, S. Santoro, D. Sheinson, J. Hung, J. M. Giltnane, A. A. Pierce, K. Mesh, S. Lianoglou, J. Riegler, R. A. D. Carano, P. Eriksson, M. Höglund, L. Somarriba, D. L. Halligan, M. S. Van Der Heijden, Y. Loriot, J. E. Rosenberg, L. Fong, I. Mellman, D. S. Chen, M. Green, C. Derleth, G. D. Fine, P. S. Hegde, R. Bourgon, T. Powles, TGFβ attenuates tumour response to PD-L1 blockade by contributing to exclusion of T cells. *Nature* **554**, 544–548 (2018).
12. Y. Zhou, I. N. Bastian, M. D. Long, M. Dow, W. Li, T. Liu, R. K. Ngu, L. Antonucci, J. Y. Huang, Q. T. Phung, X. H. Zhao, S. Banerjee, X. J. Lin, H. Wang, B. Dang, S. Choi, D. Karin, H. Su, M. H. Ellisman, C. Jamieson, M. Bosenberg, Z. Cheng, J. Haybaeck, L. Kenner, K. M. Fisch, R. Bourgon, G. Hernandez, J. R. Lill, S. Liu, H. Carter, I. Mellman, M. Karin, S. Shalapour, Activation of NF-κB and p300/CBP potentiates cancer chemoimmunotherapy through induction of MHC-I antigen presentation. *Proc. Natl. Acad. Sci. U. S. A.* **118**, e2025840118 (2021).
13. N. A. Rizvi, M. D. Hellmann, A. Snyder, P. Kvistborg, V. Makarov, J. J. Havel, W. Lee, J. Yuan, P. Wong, T. S. Ho, M. L. Miller, N. Rekhtman, A. L. Moreira, F. Ibrahim, C. Bruggeman, B. Gasmi, R. Zappasodi, Y. Maeda, C. Sander, E. B. Garon, T. Merghoub, J. D. Wolchok, T. N. Schumacher, T. A. Chan, Cancer immunology. Mutational landscape determines sensitivity to PD-1 blockade in non-small cell lung cancer. *Science* **348**, 124–128 (2015).
14. M. Yarchoan, A. Hopkins, E. M. Jaffee, Tumor mutational burden and response rate to PD-1 inhibition. *N. Engl. J. Med.* **377**, 2500–2501 (2017).
15. L. Marcus, S. J. Lemery, P. Keegan, R. Pazdur, FDA approval summary: Pembrolizumab for the treatment of microsatellite instability-high solid tumors. *Clin. Cancer Res.* **25**, 3753–3758 (2019).
16. D. J. McGrail, P. G. Pilié, N. U. Rashid, L. Voorwerk, M. Slagter, M. Kok, E. Jonasch, M. Khasraw, A. B. Heimberger, B. Lim, N. T. Ueno, J. K. Litton, R. Ferrarotto, J. T. Chang, S. L. Moulder, S. Y. Lin, High tumor mutation burden fails to predict immune checkpoint blockade response across all cancer types. *Ann. Oncol.* **32**, 661–672 (2021).
17. M. Gromeier, M. C. Brown, G. Zhang, X. Lin, Y. Chen, Z. Wei, N. Beaubier, H. Yan, Y. He, A. Desjardins, J. E. Herndon, F. S. Varn, R. G. Verhaak, J. Zhao, D. P. Bolognesi, A. H. Friedman, H. S. Friedman, F. McSherry, A. M. Muscat, E. S. Lipp, S. K. Nair, M. Khasraw, K. B. Peters, D. Randazzo, J. H. Sampson, R. E. McLendon, D. D. Bigner, D. M. Ashley, Very low mutation burden is a feature of inflamed recurrent glioblastomas responsive to cancer immunotherapy. *Nat. Commun.* **12**, 352 (2021).
18. J. H. Shim, H. S. Kim, H. Cha, S. Kim, T. M. Kim, V. Anagnostou, Y. L. Choi, H. A. Jung, J. M. Sun, J. S. Ahn, M. J. Ahn, K. Park, W. Y. Park, S. H. Lee, HLA-corrected tumor mutation burden and homologous recombination deficiency for the prediction of response to PD-(L)1 blockade in advanced non-small-cell lung cancer patients. *Ann. Oncol.* **31**, 902–911 (2020).
19. N. McGranahan, A. J. S. Furness, R. Rosenthal, S. Ramskov, R. Lyngaa, S. K. Saini, M. Jamal-Hanjani, G. A. Wilson, N. J. Birkbak, C. T. Hiley, T. B. K. Watkins, S. Shafi, N. Murugaesu, R. Mitter, A. U. Akarca, J. Linares, T. Marafioti, J. Y. Henry, E. M. Van Allen, D. Miao, B. Schilling, D. Schadendorf, L. A. Garraway, V. Makarov, N. A. Rizvi, A. Snyder, M. D. Hellmann, T. Merghoub, J. D. Wolchok, S. A. Shukla, C. J. Wu, K. S. Peggs, T. A. Chan, S. R. Hadrup, S. A. Quezada, C. Swanton, Clonal neoantigens elicit T cell immunoreactivity and sensitivity to immune checkpoint blockade. *Science* **351**, 1463–1469 (2016).
20. N. McGranahan, C. Swanton, Neoantigen quality, not quantity. *Sci. Transl. Med.* **11**, eaax7918 (2019).
21. N. Niknafs, A. Balan, C. Cherry, K. Hummelink, K. Monkhorst, X. M. Shao, Z. Belcaid, K. A. Marrone, J. Murray, K. N. Smith, B. Levy, J. Feliciano, C. L. Hann, V. Lam, D. M. Pardoll, R. Karchin, T. Y. Seiwert, J. R. Brahmer, P. M. Forde, V. E. Velculescu, V. Anagnostou, Persistent mutation burden drives sustained anti-tumor immune responses. *Nat. Med.* **29**, 440–449 (2023).
22. T. E. Keenan, K. P. Burke, E. M. Van Allen, Genomic correlates of response to immune checkpoint blockade. *Nat. Med.* **25**, 389–402 (2019).
23. J. J. Havel, D. Chowell, T. A. Chan, The evolving landscape of biomarkers for checkpoint inhibitor immunotherapy. *Nat. Rev. Cancer* **19**, 133–150 (2019).
24. S. Spranger, R. Bao, T. F. Gajewski, Melanoma-intrinsic β-catenin signalling prevents anti-tumour immunity. *Nature* **523**, 231–235 (2015).
25. M. C. V. Cormedi, E. M. Van Allen, L. M. Colli, Predicting immunotherapy response through genomics. *Curr. Opin. Genet. Dev.* **66**, 1–9 (2021).
26. F. Skoulidis, M. E. Goldberg, D. M. Greenawalt, M. D. Hellmann, M. M. Awad, J. F. Gainor, A. B. Schrock, R. J. Hartmaier, S. E. Trabucco, L. Gay, S. M. Ali, J. A. Elvin, G. Singal, J. S. Ross, D. Fabrizio, P. M. Szabo, H. Chang, A. Sasson, S. Srinivasan, S. Kirov, J. Szustakowski, P. Vitazka, R. Edwards, J. A. Bufill, N. Sharma, S.-H. I. Ou, N. Peled, D. R. Spigel, H. Rizvi, E. J. Aguilar, B. W. Carter, J. Erasmus, D. F. Halpenny, A. J. Plodkowski, N. M. Long, M. Nishino, W. L. Denning, A. Galan-Cobo, H. Hamdi, T. Hirz, P. Tong, J. Wang, J. Rodriguez-Canales, P. A. Villalobos, E. R. Parra, N. Kalhor, L. M. Sholl, J. L. Sauter, A. A. Jungbluth, M. Mino-Kenudson, R. Azimi, Y. Y. Elamin, J. Zhang, G. C. Leonardi, F. Jiang, K.-K. Wong, J. J. Lee, V. A. Papadimitrakopoulou, I. I. Wistuba, V. A. Miller, G. M. Frampton, J. D. Wolchok, A. T. Shaw, P. A. Jänne, P. J. Stephens, C. M. Rudin, W. J. Geese, L. A. Albacker, J. V. Heymach, STK11/LKB1 mutations and PD-1 inhibitor resistance in KRAS-mutant lung adenocarcinoma. *Cancer Discov.* **8**, 822–835 (2018).
27. R. W. Jenkins, R. Thummalapalli, J. Carter, I. Cañadas, D. A. Barbie, Molecular and genomic determinants of response to immune checkpoint inhibition in cancer. *Annu. Rev. Med.* **69**, 333–347 (2018).
28. W. Zhang, Y. Kong, Y. Li, F. Shi, J. Lyu, C. Sheng, S. Wang, Q. Wang, Novel molecular determinants of response or resistance to immune checkpoint inhibitor therapies in melanoma. *Front. Immunol.* **12**, 798474 (2021).
29. M. Montesion, K. Murugesan, D. X. Jin, R. Sharaf, N. Sanchez, A. Guria, M. Minker, G. Li, V. Fisher, E. S. Sokol, D. C. Pavlick, J. A. Moore, A. Braly, G. Singal, D. Fabrizio, L. A. Comment, N. A. Rizvi, B. M. Alexander, G. M. Frampton, P. S. Hegde, L. A. Albacker, Somatic HLA class I loss is a widespread mechanism of immune evasion which refines the use of tumor mutational burden as a biomarker of checkpoint inhibitor response. *Cancer Discov.* **11**, 282–292 (2021).
30. A. M. Goodman, A. Castro, R. M. Pyke, R. Okamura, S. Kato, P. Riviere, G. Frampton, E. Sokol, X. Zhang, E. D. Ball, H. Carter, R. Kurzrock, MHC-I genotype and tumor mutational burden predict response to immunotherapy. *Genome Med.* **12**, 45 (2020).
31. J. M. Zaretsky, A. Garcia-Diaz, D. S. Shin, H. Escuin-Ordinas, W. Hugo, S. Hu-Lieskovan, D. Y. Torrejon, G. Abril-Rodriguez, S. Sandoval, L. Barthly, J. Saco, B. H. Moreno, R. Mezzadra, B. Chmielowski, K. Ruchalski, I. P. Shintaku, P. J. Sanchez, C. Puig-Saus, G. Cherry, E. Seja, X. Kong, J. Pang, B. Berent-Maoz, B. Comin-Anduix, T. G. Graeber, P. C. Tumeh, T. N. M. Schumacher, R. S. Lo, A. Ribas, Mutations associated with acquired resistance to PD-1 blockade in melanoma. *N. Engl. J. Med.* **379**, 819–829 (2016).
32. A. Patterson, N. Auslander, Mutated processes predict immune checkpoint inhibitor therapy benefit in metastatic melanoma. *Nat. Commun.* **13**, 5151 (2022).
33. F. Zheng, M. R. Kelly, D. J. Ramms, M. L. Heintschel, K. Tao, B. Tutuncuoglu, J. J. Lee, K. Ono, H. Foussard, M. Chen, K. A. Herrington, E. Silva, S. N. Liu, J. Chen, C. Churas, N. Wilson,

A. Kratz, R. T. Pillich, D. N. Patel, J. Park, B. Kuenzi, M. K. Yu, K. Licon, D. Pratt, J. F. Kreisberg, M. Kim, D. L. Swaney, X. Nan, S. I. Fraley, J. S. Gutkind, N. J. Krogan, T. Ideker, Interpretation of cancer mutations using a multiscale map of protein systems. *Science* **374**, eabf3067 (2021).

34. R. M. Samstein, C. H. Lee, A. N. Shoushtari, M. D. Hellmann, R. Shen, Y. Y. Janjigian, D. A. Barron, A. Zehir, E. J. Jordan, A. Omuro, T. J. Kaley, S. M. Kendall, R. J. Motzer, A. A. Hakimi, M. H. Voss, P. Russo, J. Rosenberg, G. Iyer, B. H. Bochner, D. F. Bajorin, H. A. Al-Ahmadie, J. E. Chaft, C. M. Rudin, G. J. Riely, S. Baxi, A. L. Ho, R. J. Wong, D. G. Pfister, J. D. Wolchok, C. A. Barker, P. H. Gutin, C. W. Brennan, V. Tabar, I. K. Mellinghoff, L. M. DeAngelis, C. E. Ariyan, N. Lee, W. D. Tap, M. M. Gounder, S. P. D'Angelo, L. Saltz, Z. K. Stadler, H. I. Scher, J. Baselga, P. Razavi, C. A. Klebanoff, R. Yaeger, N. H. Segal, G. Y. Ku, R. P. DeMatteo, M. Ladanyi, N. A. Rizvi, M. F. Berger, N. Riaz, D. B. Solit, T. A. Chan, L. G. T. Morris, Tumor mutational load predicts survival after immunotherapy across multiple cancer types. *Nat Genet.* **51**, 202–206 (2019).
35. M. D. Hellmann, T. Nathanson, H. Rizvi, B. C. Creelan, F. Sanchez-Vega, A. Ahuja, A. Ni, J. B. Novik, L. M. B. Mangarin, M. Abu-Akeel, C. Liu, J. L. Sauter, N. Rekhtman, E. Chang, M. K. Callahan, J. E. Chaft, M. H. Voss, M. Tenet, X. M. Li, K. Covello, A. Renninger, P. Vitazka, W. J. Geese, H. Borghaei, C. M. Rudin, S. J. Antonia, C. Swanton, J. Hammerbacher, T. Merghoub, N. McGranahan, A. Snyder, J. D. Wolchok, Genomic features of response to combination immunotherapy in patients with advanced non-small-cell lung cancer. *Cancer Cell* **33**, 843–852.e4 (2018).
36. J. Zhang, X. Bu, H. Wang, Y. Zhu, Y. Geng, N. T. Nihira, Y. Tan, Y. Ci, F. Wu, X. Dai, J. Guo, Y. H. Huang, C. Fan, S. Ren, Y. Sun, G. J. Freeman, P. Sicinski, W. Wei, Cyclin D-CDK4 kinase destabilizes PD-L1 via cullin 3-SPOP to control cancer immune surveillance. *Nature* **553**, 91–95 (2018).
37. J. Dubrot, P. P. Du, S. K. Lane-Reticker, E. A. Kessler, A. J. Muscato, A. Mehta, S. S. Freeman, P. M. Allen, K. E. Olander, K. M. Ockerman, C. H. Wolfe, F. Wiesmann, N. H. Knudsen, H.-W. Tsao, A. Iracheta-Vellve, E. M. Schneider, A. N. Rivera-Rosario, I. C. Kohnle, H. W. Pope, A. Ayer, G. Mishra, M. D. Zimmer, S. Y. Kim, A. Mahapatra, H. Ebrahimi-Nik, D. T. Frederick, G. M. Boland, W. N. Haining, D. E. Root, J. G. Doench, N. Hacohen, K. B. Yates, R. T. Manguso, In vivo CRISPR screens reveal the landscape of immune evasion pathways across cancer. *Nat. Immunol.* **23**, 1495–1506 (2022).
38. A. Lin, Z. Qiu, J. Zhang, P. Luo, Effect of NCOR1 mutations on immune microenvironment and efficacy of immune checkpoint inhibitors in patient with bladder cancer. *Front. Immunol.* **12**, 630773 (2021).
39. S. Park, C.-Y. Ock, H. Kim, S. Pereira, S. Park, M. Ma, S. Choi, S. Kim, S. Shin, B. J. Aum, K. Paeng, D. Yoo, H. Cha, S. Park, K. J. Suh, H. A. Jung, S. H. Kim, Y. J. Kim, J.-M. Sun, J.-H. Chung, J. S. Ahn, M.-J. Ahn, J. S. Lee, K. Park, S. Y. Song, Y.-J. Bang, Y.-L. Choi, T. S. Mok, S.-H. Lee, Artificial intelligence-powered spatial analysis of tumor-infiltrating lymphocytes as complementary biomarker for immune checkpoint inhibition in non-small-cell lung cancer. *J. Clin. Oncol.* **40**, 1916–1928 (2022).
40. Cancer Genome Atlas Research Network, Comprehensive molecular profiling of lung adenocarcinoma. *Nature* **511**, 543–550 (2014).
41. Cancer Genome Atlas Research Network, Comprehensive genomic characterization of squamous cell lung cancers. *Nature* **489**, 519–525 (2012).
42. M. Sade-Feldman, Y. J. Jiao, J. H. Chen, M. S. Rooney, M. Barzily-Rokni, J. P. Eliane, S. L. Bjorgaard, M. R. Hammond, H. Vitzthum, S. M. Blackmon, D. T. Frederick, M. Hazar-Rethinam, B. A. Nadres, E. E. Van Seventer, S. A. Shukla, K. Yizhak, J. P. Ray, D. Rosebrock, D. Livitz, V. Adalsteinsson, G. Getz, L. M. Duncan, B. Li, R. B. Corcoran, D. P. Lawrence, A. Stemmer-Rachamimov, G. M. Boland, D. A. Landau, K. T. Flaherty, R. J. Sullivan, N. Hacohen, Resistance to checkpoint blockade therapy through inactivation of antigen presentation. *Nat. Commun.* **8**, 1062 (2017).
43. M. Y. Teo, K. Seier, I. Ostrovnaya, A. M. Regazzi, B. E. Kania, M. M. Moran, C. K. Cipolla, M. J. Bluth, J. Chaim, H. Al-Ahmadie, A. Snyder, M. I. Carlo, D. B. Solit, M. F. Berger, S. Funt, J. D. Wolchok, G. Iyer, D. F. Bajorin, M. K. Callahan, J. E. Rosenberg, Alterations in DNA damage response and repair genes as potential marker of clinical benefit from PD-1/PD-L1 blockade in advanced urothelial cancers. *J. Clin. Oncol.* **36**, 1685–1694 (2018).
44. R. Ramapriyan, M. S. Caetano, H. B. Barsoumian, A. C. P. Mafra, E. P. Zambalde, H. Menon, E. Tsouko, J. W. Welsh, M. A. Cortez, Altered cancer metabolism in mechanisms of immunotherapy resistance. *Pharmacol. Ther.* **195**, 162–171 (2019).
45. K. J. Lastwika, W. Wilson, Q. K. Li, J. Norris, H. Xu, S. R. Ghazarian, H. Kitagawa, S. Kawabata, J. M. Taube, S. Yao, L. N. Liu, J. J. Gills, P. A. Dennis, Control of PD-L1 expression by oncogenic activation of the AKT–mTOR pathway in non–small cell lung cancer. *Cancer Res.* **76**, 227–238 (2016).
46. T. Ohta, K. Iijima, M. Miyamoto, I. Nakahara, H. Tanaka, M. Ohtsuji, T. Suzuki, A. Kobayashi, J. Yokota, T. Sakiyama, T. Shibata, M. Yamamoto, S. Hirohashi, Loss of Keap1 function activates Nrf2 and provides advantages for lung cancer cell growth. *Cancer Res.* **68**, 1303–1309 (2008).
47. B. Ricciuti, K. C. Arbour, J. J. Lin, A. Vajdi, N. Vokes, L. Hong, J. Zhang, M. Y. Tolstorukov, Y. Y. Li, L. F. Spurr, A. D. Cherniack, G. Recondo, G. Lamberti, X. Wang, D. Venkatraman, J. V. Alessi, V. R. Vaz, H. Rizvi, J. Egger, A. J. Plodkowski, S. Khosrowjerdi, S. Digumarthy, H. Park, N. Vaz, M. Nishino, L. M. Sholl, D. Barbie, M. Altan, J. V. Heymach, F. Skoulidis, J. F. Gainor, M. D. Hellmann, M. M. Awad, Diminished efficacy of programmed death-(Ligand)1 inhibition in STK11- and KEAP1-mutant lung adenocarcinoma is affected by KRAS mutation status. *J. Thorac. Oncol.* **17**, 399–410 (2022).
48. M. M. Kaneda, K. S. Messer, N. Ralainirina, H. Li, C. J. Leem, S. Gorjestani, G. Woo, A. V. Nguyen, C. C. Figueiredo, P. Foubert, M. C. Schmid, M. Pink, D. G. Winkler, M. Rausch, V. J. Palombella, J. Kutok, K. McGovern, K. A. Frazer, X. Wu, M. Karin, R. Sasik, E. E. W. Cohen, J. A. Varner, PI3Kγ is a molecular switch that controls immune suppression. *Nature* **539**, 437–442 (2016).
49. O. De Henau, M. Rausch, D. Winkler, L. F. Campesato, C. Liu, D. H. Cymerman, S. Budhu, A. Ghosh, M. Pink, J. Tchaicha, M. Douglas, T. Tibbitts, S. Sharma, J. Proctor, N. Kosmider, K. White, H. Stern, J. Soglia, J. Adams, V. J. Palombella, K. McGovern, J. L. Kutok, J. D. Wolchok, T. Merghoub, Overcoming resistance to checkpoint blockade therapy by targeting PI3Kγ in myeloid cells. *Nature* **539**, 443–447 (2016).
50. J. Wang, M. Li, X. Han, H. Wang, X. Wang, G. Ma, T. Xia, S. Wang, MiR-1976 knockdown promotes epithelial–mesenchymal transition and cancer stem cell properties inducing triple-negative breast cancer metastasis. *Cell Death Dis.* **11**, 1–12 (2020).
51. G. S. Bova, H. M. L. Kallio, M. Annala, K. Kivinummi, G. Högnäs, S. Häyrynen, T. Rantapero, V. Kivinen, W. B. Isaacs, T. Tolonen, M. Nykter, T. Visakorpi, Integrated clinical, whole-genome, and transcriptome analysis of multisampled lethal metastatic prostate cancer. *Cold Spring Harb. Mol. Case Stud.* **2**, a000752 (2016).
52. M. Falasca, T. Maffucci, Targeting p110gamma in gastrointestinal cancers: Attack on multiple fronts. *Front. Physiol.* **5**, 391 (2014).
53. C. Torres, G. Mancinelli, J. Cordoba-Chacon, N. Viswakarma, K. Castellanos, S. Grimaldo, S. Kumar, D. Principe, M. J. Dorman, R. McKinney, E. Hirsch, D. Dawson, H. G. Munshi, A. Rana, P. J. Grippo, p110γ deficiency protects against pancreatic carcinogenesis yet predisposes to diet-induced hepatotoxicity. *Proc. Natl. Acad. Sci. U.S.A.* **116**, 14724–14733 (2019).
54. S. Zhang, W.-C. Chung, G. Wu, S. E. Egan, L. Miele, K. Xu, Manic fringe promotes a claudin-low breast cancer phenotype through notch-mediated PIK3CG induction. *Cancer Res.* **75**, 1936–1943 (2015).
55. M. K. Rathinaswamy, U. Dalwadi, K. D. Fleming, C. Adams, J. T. B. Stariha, E. Pardon, M. Baek, O. Vadas, F. DiMaio, J. Steyaert, S. D. Hansen, C. K. Yip, J. E. Burke, Structure of the phosphoinositide 3-kinase (PI3K) p110γ-p101 complex reveals molecular mechanism of GPCR activation. *Sci. Adv.* **7**, eabj4282 (2021).
56. M. K. Rathinaswamy, Z. Gaieb, K. D. Fleming, C. Borsari, N. J. Harris, B. E. Moeller, M. P. Wymann, R. E. Amaro, J. E. Burke, Disease-related mutations in PI3Kγ disrupt regulatory C-terminal dynamics and reveal a path to selective inhibitors. *Elife* **10**, e64691 (2021).
57. P. J. Brown, K. K. Wong, S. L. Felce, L. Lyne, H. Spearman, E. J. Soilleux, L. M. Pedersen, M. B. Møller, T. M. Green, D. M. Gascoyne, A. H. Banham, FOXP1 suppresses immune response signatures and MHC class II expression in activated B-cell-like diffuse large B-cell lymphomas. *Leukemia* **30**, 605–616 (2016).
58. H. Wang, J. Geng, X. Wen, E. Bi, A. V. Kossenkov, A. I. Wolf, J. Tas, Y. S. Choi, H. Takata, T. J. Day, L.-Y. Chang, S. L. Sprout, E. K. Becker, J. Willen, L. Tian, X. Wang, C. Xiao, P. Jiang, S. Crotty, G. D. Victora, L. C. Showe, H. O. Tucker, J. Erikson, H. Hu, The transcription factor Foxp1 is a critical negative regulator of the differentiation of follicular helper T cells. *Nat. Immunol.* **15**, 667–675 (2014).
59. P. De Silva, S. Garaud, C. Solinas, A. de Wind, G. Van den Eyden, V. Jose, C. Gu-Trantien, E. Migliori, A. Boisson, C. Naveaux, H. Duvillier, L. Craciun, D. Larsimont, M. Piccart-Gebhart, K. Willard-Gallo, FOXP1 negatively regulates tumor infiltrating lymphocyte migration in human breast cancer. *EBioMedicine* **39**, 226–238 (2019).
60. T. Davoli, H. Uno, E. C. Wooten, S. J. Elledge, Tumor aneuploidy correlates with markers of immune evasion and with reduced response to immunotherapy. *Science* **355**, eaaf8399 (2017).
61. S. Mohammadi, J. Davila-Velderrain, M. Kellis, Reconstruction of cell-type-specific interactomes at single-cell resolution. *Cell Syst.* **9**, 559–568.e4 (2019).
62. Y. Qin, E. L. Huttlin, C. F. Winsnes, M. L. Gosztyla, L. Wacheul, M. R. Kelly, S. M. Blue, F. Zheng, M. Chen, L. V. Schaffer, K. Licon, A. Bäckström, L. P. Vaites, J. J. Lee, W. Ouyang, S. N. Liu, T. Zhang, E. Silva, J. Park, A. Pitea, J. F. Kreisberg, S. P. Gygi, J. Ma, J. W. Harper, G. W. Yeo, D. L. J. Lafontaine, E. Lundberg, T. Ideker, A multi-scale map of cell structure fusing protein images and interactions. *Nature* **600**, 1–7 (2021).
63. T. Hart, M. Chandrashekhar, M. Aregger, Z. Steinhart, K. R. Brown, G. MacLeod, M. Mis, M. Zimmermann, A. Fradet-Turcotte, S. Sun, P. Mero, P. Dirks, S. Sidhu, F. P. Roth, O. S. Rissland, D. Durocher, S. Angers, J. Moffat, High-resolution CRISPR screens reveal fitness genes and genotype-specific cancer liabilities. *Cell* **163**, 1515–1526 (2015).
64. Y. Cai, M. J. Hossain, J.-K. Hériché, A. Z. Politi, N. Walther, B. Koch, M. Wachsmuth, B. Nijmeijer, M. Kueblbeck, M. Martinic-Kavur, R. Ladurner, S. Alexander, J.-M. Peters, J. Ellenberg, Experimental and computational framework for a dynamic protein atlas of human cell division. *Nature* **561**, 411–415 (2018).
65. L. M. Boll, J. Perera-Bel, A. Rodriguez-Vida, O. Arpí, A. Rovira, N. Juanpere, S. Vázquez Montes de Oca, S. Hernández-Llodrà, J. Lloreta, M. M. Albà, J. Bellmunt, The

impact of mutational clonality in predicting the response to immune checkpoint inhibitors in advanced urothelial cancer. *Sci. Rep.* **13**, 15287 (2023).
66. A. Mayakonda, D.-C. Lin, Y. Assenov, C. Plass, H. P. Koeffler, Maftools: Efficient and comprehensive analysis of somatic variants in cancer. *Genome Res.* **28**, 1747–1756 (2018).
67. D. R. Cox, Regression models and life-tables. *J. R. Stat. Soc. Ser. B* **34**, 187–202 (1972).
68. H. Ishwaran, U. B. Kogalur, E. H. Blackstone, M. S. Lauer, Random survival forests. *Ann. Appl. Stat.* **2**, 841–860 (2008).
69. C. Davidson-Pilon, Lifelines: Survival analysis in Python. *J. Open Source Softw.* **4**, 1317 (2019).
70. S. Pölsterl, Scikit-survival: A library for time-to-event analysis built on top of scikit-learn. *J. Mach. Learn. Res.* **21**, 1–6 (2020).
71. R. T. Pillich, J. Chen, C. Churas, D. Fong, B. M. Gyori, T. Ideker, K. Karis, S. N. Liu, K. Ono, A. Pico, D. Pratt, NDEx IQuery: A multi-method network gene set analysis leveraging the network data exchange. *Bioinformatics* **39**, btad118 (2023).
72. K. Hanspers, A. Riutta, M. Summer-Kutmon, A. R. Pico, Pathway information extracted from 25 years of pathway figures. *Genome Biol.* **21**, 273 (2020).
73. E. Cerami, J. Gao, U. Dogrusoz, B. E. Gross, S. O. Sumer, The cBio cancer genomics portal: An open platform for exploring multidimensional cancer genomics data. *Cancer Discov.* **2**, 401–404 (2012).
74. J. Gao, B. A. Aksoy, U. Dogrusoz, G. Dresdner, B. Gross, S. O. Sumer, Y. Sun, A. Jacobsen, R. Sinha, E. Larsson, E. Cerami, C. Sander, N. Schultz, Integrative analysis of complex cancer genomics and clinical profiles using the cBioPortal. *Sci. Signal.* **6**, l1 (2013).
75. A. Colaprico, T. C. Silva, C. Olsen, L. Garofano, C. Cava, D. Garolini, T. S. Sabedot, T. M. Malta, S. M. Pagnotta, I. Castiglioni, M. Ceccarelli, G. Bontempi, H. Noushmehr, TCGAbiolinks: An R/Bioconductor package for integrative analysis of TCGA data. *Nucleic Acids Res.* **44**, e71 (2016).
76. D. Pratt, J. Chen, D. Welker, R. Rivas, R. Pillich, V. Rynkov, K. Ono, C. Miello, L. Hicks, S. Szalma, A. Stojmirovic, R. Dobrin, M. Braxenthaler, J. Kuentzer, B. Demchak, T. Ideker, NDEx, the network data exchange. *Cell Syst.* **1**, 302–305 (2015).
77. N. Hartman, S. Kim, K. He, J. D. Kalbfleisch, Pitfalls of the concordance index for survival outcomes. *Stat. Med.* **42**, 2179–2190 (2023).
78. B. Jassal, L. Matthews, G. Viteri, C. Gong, P. Lorente, A. Fabregat, K. Sidiropoulos, J. Cook, M. Gillespie, R. Haw, F. Loney, B. May, M. Milacic, K. Rothfels, C. Sevilla, V. Shamovsky, S. Shorser, T. Varusai, J. Weiser, G. Wu, L. Stein, H. Hermjakob, P. D'Eustachio, The reactome pathway knowledgebase. *Nucleic Acids Res.* **48**, D498–D503 (2020).
79. H. Mi, A. Muruganujan, D. Ebert, X. Huang, P. D. Thomas, PANTHER version 14: More genomes, a new PANTHER GO-slim and improvements in enrichment analysis tools. *Nucleic Acids Res.* **47**, D419–D426 (2019).
80. Q. He, C. Sun, Y. Pan, Whole-exome sequencing reveals Lewis lung carcinoma is a hypermutated Kras/Nras–mutant cancer with extensive regional mutation clusters in its genome. *Sci. Rep.* **14**, 1–14 (2024).
81. J. G. Doench, E. Hartenian, D. B. Graham, Z. Tothova, M. Hegde, I. Smith, M. Sullender, B. L. Ebert, R. J. Xavier, D. E. Root, Rational design of highly active sgRNAs for CRISPR-Cas9–mediated gene inactivation. *Nat. Biotechnol.* **32**, 1262–1267 (2014).
82. A. Subramanian, P. Tamayo, V. K. Mootha, S. Mukherjee, B. L. Ebert, M. A. Gillette, A. Paulovich, S. L. Pomeroy, T. R. Golub, E. S. Lander, J. P. Mesirov, Gene set enrichment analysis: A knowledge-based approach for interpreting genome-wide expression profiles. *Proc. Natl. Acad. Sci. U. S. A.* **102**, 15545–15550 (2005).
83. Z. Fang, X. Liu, G. Peltz, GSEApy: A comprehensive package for performing gene set enrichment analysis in Python. *Bioinformatics* **39**, btac757 (2023).
84. V. Thorsson, D. L. Gibbs, S. D. Brown, D. Wolf, D. S. Bortone, T. H. O. Yang, E. Porta-Pardo, G. F. Gao, C. L. Plaisier, J. A. Eddy, E. Ziv, A. C. Culhane, E. O. Paull, I. K. A. Sivakumar, A. J. Gentles, R. Malhotra, F. Farshidfar, A. Colaprico, J. S. Parker, L. E. Mose, N. S. Vo, J. Liu, Y. Liu, J. Rader, V. Dhankani, S. M. Reynolds, R. Bowlby, A. Califano, A. D. Cherniack, D. Anastassiou, D. Bedognetti, A. Rao, K. Chen, A. Krasnitz, H. Hu, T. M. Malta, H. Noushmehr, C. S. Pedamallu, S. Bullman, A. I. Ojesina, A. Lamb, W. Zhou, H. Shen, T. K. Choueiri, J. N. Weinstein, J. Guinney, J. Saltz, R. Holt, C. E. Rabkin; The Cancer Genome Atlas Research Network, A. J. Lazar, J. S. Serody, E. G. Demicco, M. L. Disis, B. G. Vincent, L. Shmulevich, The immune landscape of cancer. *Immunity* **48**, 812–830.e14 (2018).
85. J. A. Joyce, D. T. Fearon, T cell exclusion, immune privilege, and the tumor microenvironment. *Science* **348**, 74–80 (2015).
86. L.-C. Chen, G. Papandreou, F. Schroff, H. Adam, Rethinking atrous convolution for semantic image segmentation. arXiv:1706.05587 [cs.CV] (2017).
87. K. He, X. Zhang, S. Ren, J. Sun, Deep residual learning for image recognition. arXiv:1512.03385 [cs.CV] (2015).
88. M. Amgad, E. S. Stovgaard, E. Balslev, J. Thagaard, W. Chen, S. Dudgeon, A. Sharma, J. K. Kerner, C. Denkert, Y. Yuan, K. AbdulJabbar, S. Wienert, P. Savas, L. Voorwerk, A. H. Beck, A. Madabhushi, J. Hartman, M. M. Sebastian, H. M. Horlings, J. Hudeček, F. Ciompi, D. A. Moore, R. Singh, E. Roblin, M. L. Balancin, M.-C. Mathieu, J. K. Lennerz, P. Kirtani, I.-C. Chen, J. P. Braybrooke, G. Pruneri, S. Demaria, S. Adams, S. J. Schnitt, S. R. Lakhani, F. Rojo, L. Comerma, S. S. Badve, M. Khojasteh, W. F. Symmans, C. Sotiriou, P. Gonzalez-Ericsson, K. L. Pogue-Geile, R. S. Kim, D. L. Rimm, G. Viale, S. M. Hewitt, J. M. S. Bartlett, F. Penault-Llorca, S. Goel, H.-C. Lien, S. Loibl, Z. Kos, S. Loi, M. G. Hanna, S. Michiels, M. Kok, T. O. Nielsen, A. J. Lazar, Z. Bago-Horvath, L. F. S. Kooreman, J. A. W. M. van der Laak, J. Saltz, B. D. Gallas, U. Kurkure, M. Barnes, R. Salgado, L. A. D. Cooper; International Immuno-Oncology Biomarker Working Group, Report on computational assessment of tumor infiltrating lymphocytes from the international immuno-oncology biomarker working group. *NPJ Breast Cancer* **6**, 16 (2020).
89. D. S. Chen, I. Mellman, Elements of cancer immunity and the cancer–immune set point. *Nature* **541**, 321–330 (2017).
90. F. Pedregosa, G. Varoquaux, A. Gramfort, V. Michel, B. Thirion, O. Grisel, M. Blondel, P. Prettenhofer, R. Weiss, V. Dubourg, J. Vanderplas, A. Passos, D. Cournapeau, M. Brucher, M. Perrot, É. Duchesnay, Scikit-learn: Machine learning in Python. *J. Mach. Learn. Res.* **12**, 2825–2830 (2011).
91. S. M. Lundberg, S.-I. Lee. A unified approach to interpreting model predictions, in *Advances in Neural Information Processing Systems 30* (NIPS, 2017), pp. 4768–477.
92. Plotly Technologies Inc., *Collaborative Data Science* (Plotly Technologies Inc., 2015).

Acknowledgments: We thank all of the members of the Ideker laboratory for discussions. We also acknowledge the wealth of data generated by the TCGA Research Network (www.cancer.gov/tcga). **Funding:** This research was funded by grants from the National Institutes of Health (T32CA121938 to J.K. and R01CA270437 to J.S.) and the United States National Cancer Institute (NCI grants R01CA269919 to H.C., U54CA274502 to T.I., and R01ES014811 to T.I.). **Author contributions:** J.K., X.Z., A.S., H.C., and T.I. designed the project. J.K., X.Z., A.S., S.P., R.B., J.S., H.Z., J.M., C.A., C.-Y.O., H.C., and T.I. analyzed the data and wrote the manuscript. **Competing interests:** T.I. is a cofounder, a member of the advisory board, and has an equity interest in Data4Cure and Serinus Biosciences. T.I. is a consultant for and has an equity interest in Ideaya BioSciences and Light Horse Therapeutics. The terms of these arrangements have been reviewed and approved by UC San Diego in accordance with its conflict of interest policies. J.M. and C.A. are employees at Lunit. C.-Y.O. holds a leadership role and is a stockholder at Lunit. The other authors declare that they have no competing interests. **Data and materials availability:** All data needed to evaluate the conclusions in the paper are present in the paper and/or the Supplementary Materials. Mutation and clinical datasets used in this study can be downloaded from the cBioPortal database (*73*, *74*): Samstein cohort (*34*) (www.cbioportal.org/study?id=tmb_mskcc_2018), Hellmann cohort (*35*) (www.cbioportal.org/study/summary?id=nsclc_mskcc_2018), and IMvigor210 cohort (*11*) (http://research-pub.gene.com/IMvigor210CoreBiologies). The Cancer Genome Atlas (TCGA) dataset for lung adenocarcinoma (*40*) and lung squamous cell carcinoma (*41*) can be downloaded using the TCGAbiolinks R package (*75*). The in vivo CRISPR screening data were downloaded from the corresponding publication (*37*) (www.tumorimmunity.org). The NeST hierarchy of protein assemblies (*33*) was downloaded from the Network Data Exchange (NDEx) (*76*). Analysis codes generated in the course of this research are available via Zenodo (https://zenodo.org/doi/10.5281/zenodo.11222897) or GitHub repositories (https://github.com/JungHoKong/Immunotherapy_AMB).

Submitted 29 February 2024
Accepted 13 August 2024
Published 20 September 2024
10.1126/sciadv.ado9746